Chemistry & Biology 13, 771–778, July 2006 ©2006 Elsevier Ltd All rights reserved DOI 10.1016/j.chembiol.2006.05.014

Generation and Structural Analysis of Reactive Empty Particles Derived from an Icosahedral Virus

Wendy F. Ochoa,[1] Anju Chatterji,[1] Tianwei Lin,[1] and John E. Johnson[1,2,*]
[1]Department of Molecular Biology and Center for Integrative Molecular Biosciences
The Scripps Research Institute
10550 North Torrey Pines Road
La Jolla, California 92037

Summary

Chemical and genetic modifications on the surface of viral protein cages confer unique properties to the virus particles with potential nano and biotechnological applications. The enclosed space in the interior of the virus particles further increases its versatility as a nanomaterial. In this paper, we report a simple method to generate a high yield of stable cowpea mosaic virus (CPMV) empty capsids from their native nucleoprotein counterparts by removing the encapsidated viral genome without compromising the integrity of the protein coat. Biochemical and structural comparison of artificially generated empty particles did not reveal any distinguishable differences from CPMV particles containing viral RNA. Preliminary results on the use of artificially produced empty CPMV capsids as a carrier capsule are described.

Introduction

Biological macromolecules, and in particular viral protein cages, due to their versatility, propensity to form arrays, and programmability through genetic engineering, are exceptional substrates for material synthesis and scaffolds for the self-assembly of small molecules in designed patterns [1–7].

Cowpea mosaic virus (CPMV) is a picorna-like plant virus that encapsulates two segments of single-stranded, positive sense RNA. The larger RNA1 encodes the virus replication machinery, and the smaller RNA2 encodes the capsid proteins and the viral movement protein [8]. The two RNA molecules are separately encapsidated in isometric particles, and both types of particles are required for the infection. In a sucrose gradient, CPMV can be separated into three components (Figure 1A). The bottom band, B component, is formed by the virus capsid containing the larger RNA1; the middle (M) component is that with RNA2. The top (T) components are CPMV capsids that naturally assemble without RNA.

Recent studies using structure-based engineering have demonstrated potential applications of CPMV in the area of virus-based nanomaterials. Theses studies established chemical addressability of the viral capsid via the introduction of unique Cys and Lys residues [9–11] which were selectively modified to display fluorophores, metal complexes, and even full-length proteins [12]. The affinity of thiol groups for gold was utilized to pattern colloidal gold particles on the viral template [13] that were subsequently connected by electronic molecules (nanowires) for electrical conductivity through the virus [14]. An additional utility to the virus scaffold was added by conferring metal binding properties on the capsid surface with the incorporation of short histidine-rich peptides [15] on the capsid. The crystals of CPMV were also shown to be potential substrates for engineering to use as templates for electroless plating to produce perforated metallic blocks with applications in catalysis and photonics [16].

Unlike the modifications on the exterior surface of the viral capsid, the interior surface and space have not been exploited as extensively, primarily due to the limitations imposed by the viral genome. The yield of naturally occurring empty capsids produced during the course of a natural infection cycle is less than 10% [8], thus restricting its utility. In addition, CPMV cannot efficiently assemble into mature capsids in vitro [17], like the other virus-derived nanocages (e.g., cowpea chlorotic mottle virus) that have been successfully used as reaction vessels and "nanocontainers" [18] by virtue of their ability to assemble into virus-like particles [19] in vitro.

To complement the functionalities incorporated on the exterior surface of the virus capsid with potentially useful cargo that could be encapsulated in the interior of the same particle, we looked for strategies that would allow removal of the virus nucleic acid without degradation of its protein shell. In this paper, we demonstrate the development of a simple chemical method to generate a good yield of empty capsids from nucleoprotein components by gradual hydrolysis of the viral nucleic acid. Further, these artificially generated empty capsids were compared and characterized with the natural empty particles using a combination of biochemical and structural techniques.

Results and Discussion

Excavation of Nucleic Acid from CPMV Nucleoprotein Components

Previous studies in our laboratory indicated that viral RNA was rapidly hydrolyzed when CPMV was placed under alkaline conditions. In order to identify conditions under which the viral RNA is sufficiently fragmented to diffuse from the capsid, MIX components (a mixture of RNA-containing middle and bottom capsids) were incubated in an alkaline solution of 0.05 M sodium borate (pH ranging from 8.5 to 9.4) at 37°C and room temperature. The artificial top (AT) component was isolated by ultracentrifugation in a 10%–40% sucrose gradient. Under normal conditions, the CPMV components can be resolved as three distinct bands on a sucrose gradient (Figure 1A). Samples incubated at pH 8.8–9.4 showed the accumulation of AT component, and there was no significant AT components generated at pH 8.5 (data not shown). Genomic RNA degraded gradually over time at pH 9.0, resulting in the accumulation of the AT

*Correspondence: jackj@scripps.edu
[2]Lab address: http://johnsonlab.scripps.edu/

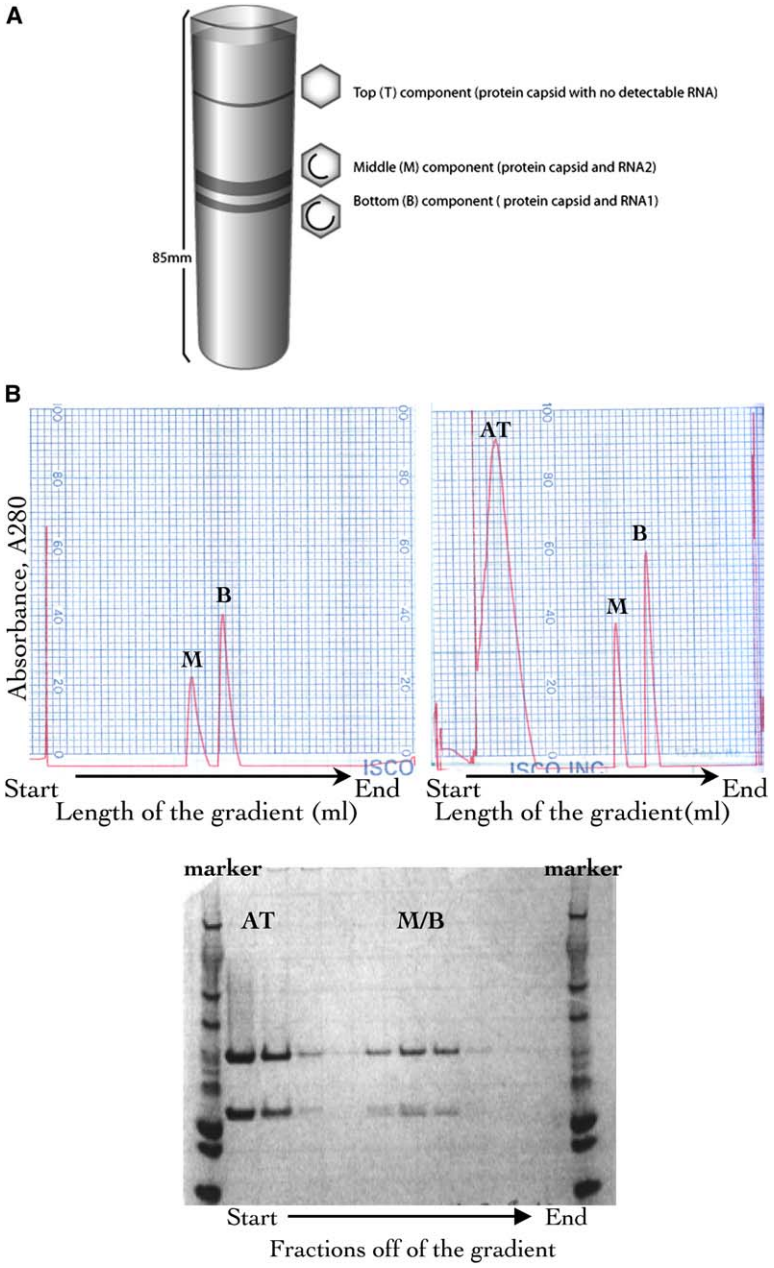

Figure 1. Characterization of CPMV Components

(A) Schematic of the CPMV component separation on a sucrose gradient (10%–40%). Three distinct virus particles with different RNA content form separate bands in a sedimentation gradient. The virus particles with no detectable RNA (top component, T) sit at the top of the gradient. T top component constitutes less than 10% of the total population in natural plant infections.

(B) Production and characterization of artificial empty particles. Upper panel: the chromatogram on the left shows the sucrose gradient fractionation profile of the MIX population after treatment at high pH that resolves into the middle (M) and bottom (B) components. The chromatogram on the right shows the accumulation of the artificially generated top component (AT) that is notably absent in particles before exposure to alkaline pH (left). Lower panel: analysis of the fractions collected off of the sucrose gradient on an SDS-PAGE gel (NuPAGE) to detect the virus capsids. Half-milliliter fractions were collected as the gradient was fractionated and alternate fractions were analyzed on an SDS-PAGE gel for the presence of virus-specific capsids. Lanes 1–3 represent the AT capsids while the residual M and B components appear later in the gradient in lanes 5–7.

component. Sucrose gradient fractionation profile showed accumulation of AT component that was concentrated in the first three (F1–F3) fractions of the gradient (Figure 1B) after resolving the fractions on an SDS-PAGE gel. Prolonged accumulation (over 4 hr at 37°C) resulted in the appearance of pentamers that arise due to the disruption of the capsid as evidenced by electron microscopy (data not shown).

Characterization of Artificially Generated Empty Capsids

The AT capsids were analyzed by ion exchange (MonoQ) and size exclusion (Superose 6) chromatography. The elution parameters of the empty capsid (22 min with a flow rate of 0.4 ml/min in size exclusion chromatography) were similar to that of wild-type CPMV. Ion exchange chromatography was performed using 50 mM phosphate buffer (pH 7.0) as the low-salt buffer and 50 mM phosphate with 1.0 M NaCl (pH 7.0) as the high-salt eluant. The retention time (38%–40% of high-salt buffer) and the elution profile of the artificial empty capsids were similar to that of wild-type empty capsids. This indicated that the surface properties of the AT capsids were not altered as a result of the alkaline pH and temperature conditions that the samples were subjected to (Figure 2).

The maximum yields of AT component were obtained by treating the CPMV particles with sodium borate at pH 9.0 overnight, followed by an additional incubation at 37°C for 5 min.

Analysis of RNA Content in AT Components

To determine the presence of residual RNA within the AT particles, the purified preparations were treated with

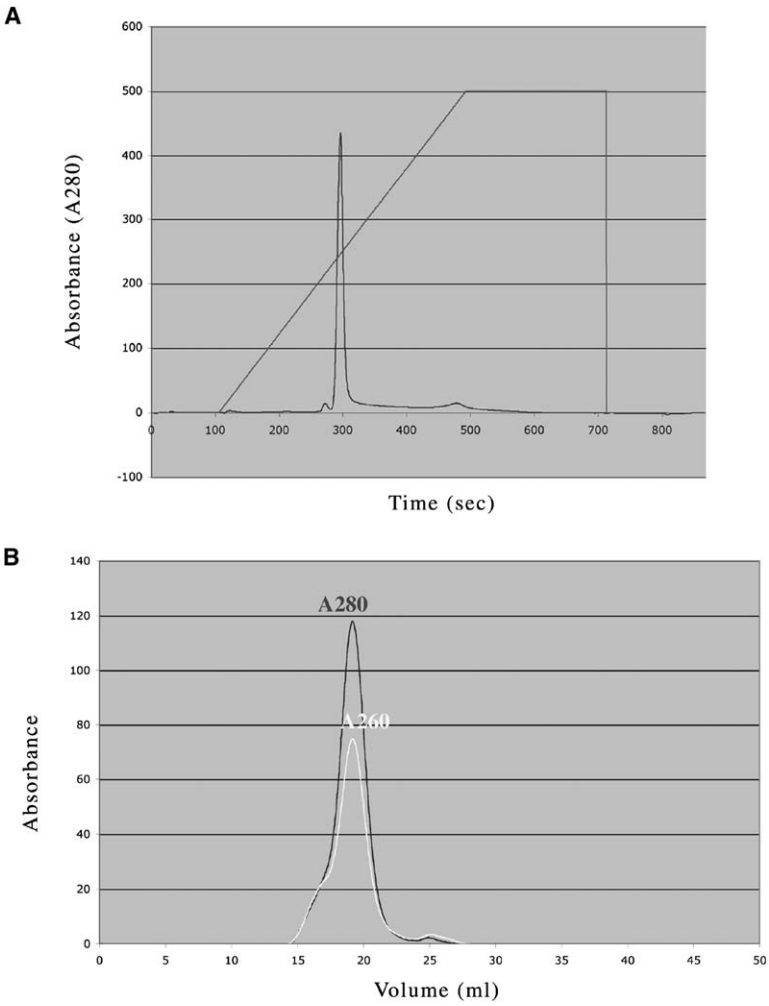

Figure 2. Characterization of AT Capsids

(A) Ion exchange chromatogram of the AT capsid. The virus capsid was eluted off of an anion exchange column using a 0–1 M salt gradient.

(B) Size exclusion chromatography of the AT component on a Superose 6 column. The increased absorbance at 280 nm instead of 260 nm indicates the absence of RNA in AT capsids.

thiazole orange (TO), a nucleic acid-specific dye that intercalates with the purines and pyrimidines. The uptake of the dye was monitored over a period of 3 hr and the kinetics of dye association with the particles was studied. Our initial experiments with the AT capsids revealed substantial amounts of dye incorporation, indicating that a significant amount of nucleic acid was still present. To determine whether the viral RNA was encapsidated and retained in the capsid interior or whether it represented hydrolyzed RNA that exited the capsid but was still associated with the capsid nonspecifically, the samples were treated with RNase A and subsequently analyzed by agarose gel electrophoresis. It was shown that the viral RNA was partially hydrolyzed prior to treatment with RNase A and formed a smear at the bottom of the lane in the electrophoresis (Figure 3A). Addition of RNase A to these samples followed by purification on Sephadex spin columns (Bio-Rad) resulted in the disappearance of the smear. No detectable amount of TO dye uptake was observed in the RNase A-treated samples (Figure 3B). These results suggested that the viral RNA was partially degraded by the alkaline treatment but substantial amounts of it were still associated with the capsid on the exterior. This residual hydrolyzed RNA was subsequently removed by treatment with RNase A.

Structural Characterization of CPMV Components

X-Ray Crystallography

Cubic crystals of T component of CPMV were obtained under identical conditions as used previously for other CPMV components. The 2.8 Å protein model determined from virions was used as the starting model for the structure determination of empty capsids. The 4 Å electron density of empty capsids was identical to the one described for the nucleoprotein component, as no RNA was visible in that structure. The structures of empty and nucleoprotein components were indistinguishable at this resolution.

Conventional Microscopy

Following the thermochemical treatment, the AT samples were purified on sucrose density gradients, concentrated to 2 mg/ml, and stained with 2% uranyl acetate. In the absence of RNA, the stain penetrates the capsid and the empty particles appeared as hollow spheres while the nucleoprotein components appeared as solid spheres. All the particles showed the same icosahedral shells. More than 95% of the AT particles observed under the transmission electron microscopy appeared intact, regular, and devoid of any RNA. This was consistent with the size exclusion chromatography and the results observed with TO dye studies.

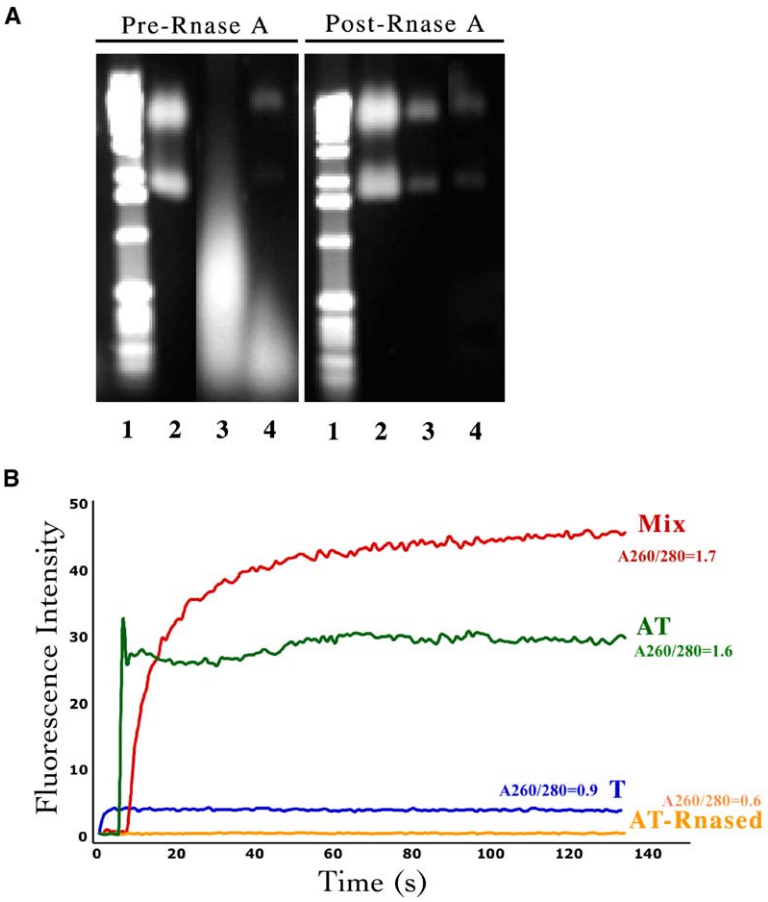

Figure 3. RNase A-Treated AT Capsids

(A) Fractions corresponding to the AT were pooled and treated with RNase A at room temperature for 30 min and analyzed on 1% agarose gels. The bands were visualized by staining the gel with SYBR green. The samples pre- and posttreatment with RNase A are indicated. Lane 1: 1 kb DNA ladder; lane 2: control, native top from wild-type CPMV; lane 3: AT fraction 3 from the sucrose gradient; lane 4: AT fraction 4 from the sucrose gradient.

(B) Kinetics of thiazole orange (TO) uptake by different virus components was measured over a period of time. The A260/280 ratio of the different components is indicated as a measure of the nucleic acid to protein content. The AT capsid bound substantial amounts of dye prior to the RNase treatment that was completely eliminated after the nuclease treatment. The native top (T) and the AT (after the RNase treatment) bound comparable amounts of TO dye.

Cryo-Electron Microscopy and Image Reconstructions

The M and T components were rapidly frozen in liquid ethane and analyzed on a Philips Tecnai F20 transmission electron microscope operating at 120 kV. Figure 4 presents the digital images collected using low-irradiation procedures (~10 e^{-}/Å^2) at a nominal magnification of 50,000 and defocus ranging between 0.8 and 1.2. Sets containing each type of particle, solid and hollow spheres, were manually selected and 20 Å resolution

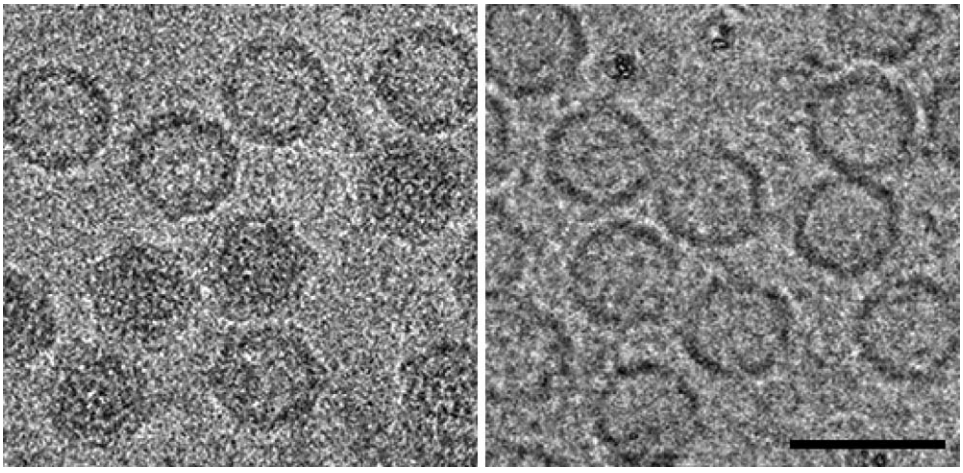

Figure 4. Electron Micrographs of Unstained, Frozen Hydrated Samples of CPMV

Left: a sample containing both nucleoprotein capsids (MIX) and natural top component (T). Right: a sample of artificial empty CPMV (AT). The scale bar represents 50 nm. The particles are readily distinguishable and easily selected. AT was obtained by a combination of high pH and heat treatment of the MIX component. After the RNA hydrolysis the capsid seems to conserve the original icosahedral shape, and appears as well-distributed hollow shells.

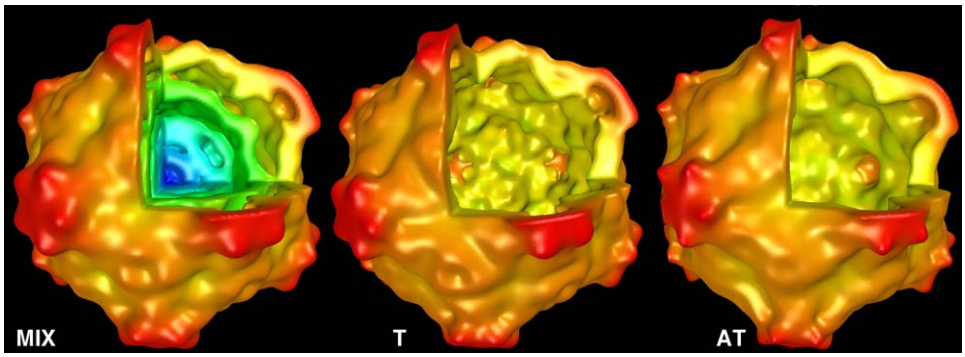

Figure 5. Three-Dimensional Structure of MIX Component, T Component, and AT Component of CPMV

Shown are surface representations of the cryo-electron microscopy maps calculated, with the top quarter cut away and colored by radius. The color representation is radially color coded from blue at the center through yellow, green, and red at the exterior. The RNA-containing region appears blue and as we move away from the center the capsid appears green, yellow, and at its highest point seems red in color.

electron density maps of the M and T components were computed from 260 and 165 individual particles, respectively (Figures 5A and 5B).

The same procedure was followed to obtain a three-dimensional structure of the AT particles. The sample was pretreated with RNase A in order to eliminate any residual RNA and enhance the homogeneity of the preparation. The final density map was calculated from 484 individual particles, with the structure of the T components as the starting model (Figure 5C).

To assess the resolution of the electron maps, each data set was divided in half to compute two independent reconstructions [20, 21]. Crosscorrelation analysis indicated that the effective resolution limit was 20–22 Å, using a cutoff of 0.5 for all three reconstructions. This was a conservative estimate, as the final map was computed from twice as many particles.

Comparison of the Capsids

The images of the M and the T components were morphologically indistinguishable based on the external features of the two capsids (Figure 5). Central sections of the maps showed the density corresponding to the RNA in the interior of the M component and a clearly empty shell for the T component (Figure 6A, upper panel). A difference map calculated by subtracting the T capsid from the M capsid showed an almost spherical electron density with a radius of 185 Å that corresponds to the virus genome. The icosahedral appearance of the density is due to the constraints imposed during the reconstruction (Figure 6A, lower panel).

To compare the interior surfaces of the M and T components, an electron density map with resolution cutoff at 20 Å was computed using the X-ray coordinates of wild-type CPMV (Protein Data Bank ID code 1NY7). The difference map calculated by subtracting this map from the electron microscopy (EM) reconstruction of the T component showed few regions of weak and random density. Both the X-ray model and the EM reconstruction showed an interior of the capsid with the same general features and no redistribution of the density was observed, indicating the absence of nucleic acid. These observations confirmed that the T component does not encapsidate any genomic RNA.

A comparison of the EM density maps of the T and AT capsids revealed that there were no significant differences between them (Figure 5). This was further confirmed by computing a difference map of the two EM reconstructions (Figure 6B). The exteriors of the capsids were indistinguishable and there was no evidence of any nucleic acid-derived density distribution in the interior of the shells.

Applications of the Empty Capsids

Empty CPMV can be used as a carrier for a variety of cargos. This was demonstrated by loading the particles with fluorescent dye molecules (model cargo), which bind to the otherwise inaccessible cysteine residues (Figure 7). There are no exposed cysteines on the exterior surface of the CPMV capsid, and even though there are 12 internal cysteines, almost all of them are buried and inaccessible due to the presence of the viral genome. We verified the availability of these internal cysteine residues for chemical reactions by attempting to address them with cysteine-specific reporter dyes. Figure 7A shows specific labeling of the AT capsids with fluorescent dyes, indicating that these empty capsids are accessible and reactive as demonstrated by the SDS-PAGE analysis of the labeled capsids under UV light (Figure 7A, left) and after staining with Coomassie brilliant blue (Figure 7A, right). The AT components appeared strongly fluorescent in comparison to the MIX nucleoprotein components, suggesting better dye incorporation. The Cy5-labeled capsids do not show up well under the UV light because their emission wavelengths are in the visible region of the spectrum. The relative numbers of the fluorescent probes incorporated into the capsids were quantitated based upon their absorbance and are represented in Figure 7B, confirming the dye labeling trend that was observed under UV illumination.

These studies indicate that CPMV-derived AT capsids can potentially serve as nanocontainers to load specific substrates into the capsid for applications ranging from chemical reactions to therapeutic payloads for drug delivery. The utility of these artificially generated particles could be further enhanced if their shelf life could be prolonged to greater than 7–10 days, possibly by optimizing the ionic strength of the resuspension buffer.

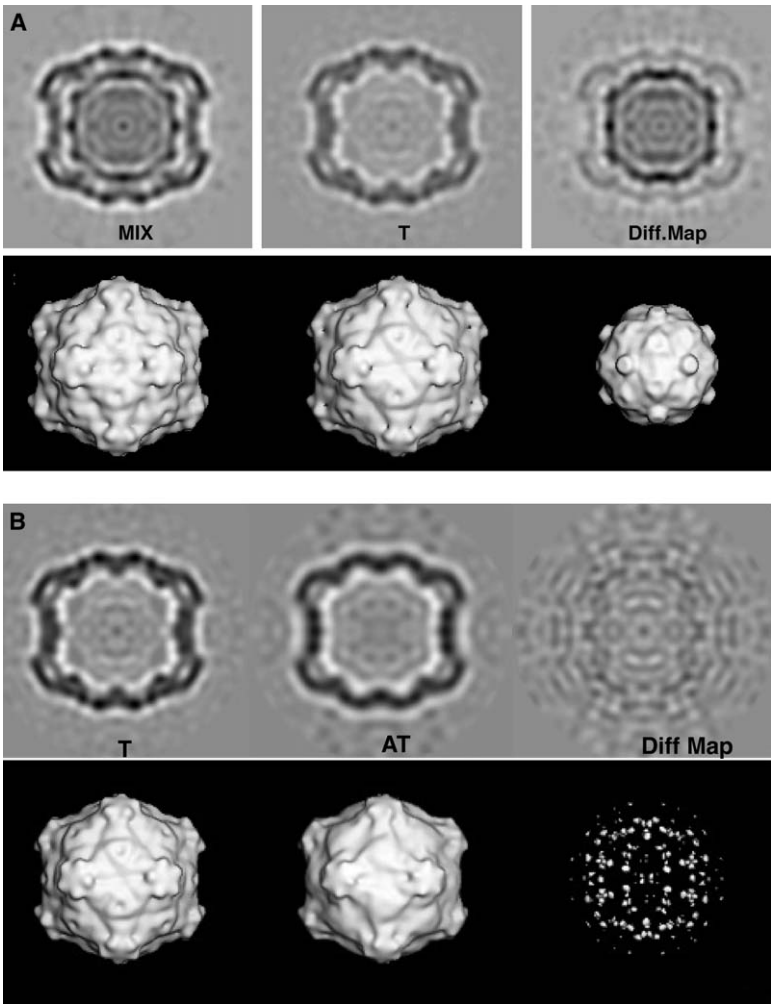

Figure 6. Difference Electron Density Maps of CPMV Components

(A) Representation of the difference map calculated by subtracting the electron density of the T capsid from the MIX component. Transverse central sections (upper panels) and surface representations (lower panel) of the maps used in the subtraction calculations with the resultant difference map.

(B) Representation of the difference map calculated by subtracting the electron density of the AT capsid from the T component. Transverse central sections (upper panel) and surface representations (lower panel) of the maps used in the subtraction calculations and the resultant difference map. The highest residual density of the difference map has almost negligible (noise) value, indicating that both capsids are basically similar and neither of them contains extra residual density in the interior of the capsid.

Significance

With this work, we have added another aspect to the utility of CPMV particles in the rapidly advancing field of nanomaterials. The chemical method described here generates a high yield of stable, empty virus particles from the nucleoprotein components. The production method is simple and unique in its ability to keep the protein coat of the particles intact and allows for scalability.

The dual modality achieved in terms of the availability of an addressable interior of the cavity as well as the ability to incorporate functionalities on the external surface greatly enhances the usefulness of our virus-based platform for nanotechnological applications.

Experimental Procedures

Propagation of the Virus in Plants

The primary leaves of cowpea seedlings were mechanically inoculated with 10 μg each of cDNA plasmids encoding RNA1 (pCP1) and RNA2 (pCP2). The initial progeny of native CPMV was extracted from infected leaves with 0.1 M potassium phosphate (pH 7.0) (phosphate buffer) 7 days postinfection. Typically, 50 plants were infected with the plant extract and the symptomatic leaves were harvested after 3 weeks. The virus was isolated according to the standard protocol [22].

Generation of Artificial Empty Capsids by Degradation of Genomic RNA

The middle and the bottom components of CPMV purified after sucrose gradients were pooled as the MIX component and dialyzed overnight in 0.1 M sodium borate buffer (pH 9.4). The dialyzed samples were further subjected to a brief heat shock at 37°C for 10 min following which the samples were immediately diluted and neutralized in 0.1 M phosphate buffer and 0.15 M sodium chloride. The neutralized samples were resolved on a 10%–40% sucrose gradient and separated using an ISCO UV gradient fractionator into 1 ml fractions. The fractions were analyzed on 4%–12% bis-Tris (NuPAGE) gels and the fractions corresponding to peaks 1 and 2 were pooled and dialyzed against 0.1 M PBS (pH 7.0) to remove sucrose and pelleted at 42,000 rpm at 4°C in a 50.2 Ti rotor (Beckman-Coulter). The empty capsids produced by the removal of the nucleic acids from the nucleoprotein components are called the artificial top (empty, AT) component.

Characterization of Artificial Empty Capsids by Chromatography

Purified virus preparations of AT particles were analyzed by size exclusion (Superose 6) and ion exchange (MonoQ) chromatography using the AKTA explorer (Amersham Pharmacia Biotech). Ion exchange chromatography was also performed using 50 mM phosphate buffer (pH 7.0) as the low-salt buffer and 50 mM phosphate with 1.0 M NaCl (pH 7.0) as the high-salt eluant as described before [11].

X-Ray Crystallography of the T Component

Sample preparation, crystallization, and data collection were previously described [23]. Data reduction, averaging, and phase

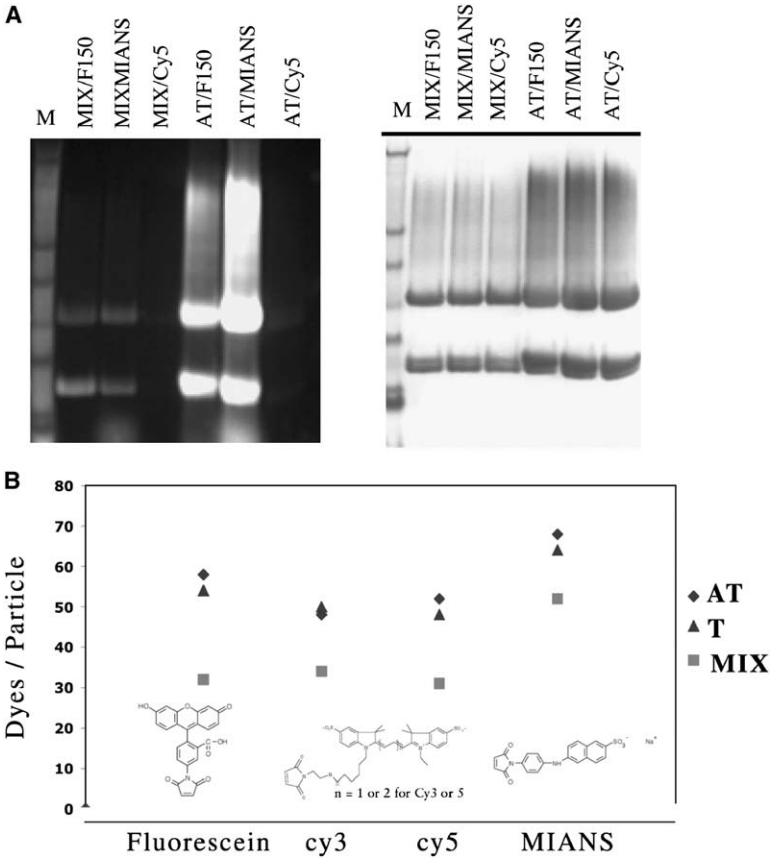

Figure 7. Labeling of Internal Cysteines

(A) The accessibility of the internal cysteines as a result of the RNA removal was confirmed with specific labeling with fluorophores. The left panel shows the SDS-PAGE gel upon illumination with UV light and the right-hand panel depicts the same gel after staining with Coomassie brilliant blue. The lanes are labeled to show the viral components derivatized with appropriate cysteine-specific fluorophores.

(B) Relative loading of the AT with fluorescent dyes. As expected, the AT and the T encapsulate a greater number of dyes than the filled (MIX) capsids.

refinement were carried out by using the CCP4 package [24]. The electron density was improved by averaging with the 5-fold noncrystallographic symmetry and the resolution was extended in steps to 4 Å resolution. CPMV coordinates corresponding to the structure of the nucleoprotein crystal structure [25] were used as a starting model and then refined according to the averaged electron density map calculated.

Conventional Electron Microscopy

Samples (8 μl) of the different fractions were applied to glow-discharged carbon-coated grids for 2 min and stained with 2% (w/v) uranyl acetate. Micrographs were recorded with a Philips CM120 microscope operating at 100 kV at a nominal magnification of 60,000×.

Cryo-Electron Microscopy and Image Reconstruction

CPMV samples were prepared by purification of the virus in a sucrose gradient. The samples were pelleted and suspended in 50 mM phosphate (pH 7.5) at a concentration of about 2–3 mg/ml. Drops (4 μl) of sample were applied to glow-discharged Quantifoil EM grids which were then blotted and plunged into a bath of liquid ethane (−180°C) using Vitrobot from FEI. Grids were transferred from liquid nitrogen to a precooled specimen holder (Gatan) that maintained the frozen hydrated sample at −184°C in a Philips Tecnai F20 transmission electron microscope. Digital images were recorded using low-irradiation procedures (~10 $e^{-}/Å^{2}$) and those that displayed minimal astigmatism and drift as assessed by visual inspection and diffraction were selected for further analysis. Particles clearly separated from neighbors or background contamination were selected and masked as individual images using the software ROBEM [21]. The image intensity values were adjusted to remove linear background gradients [26] and to normalize the means and variances of the data [27]. The initial orientation and origin parameters of the images for the reconstruction were determined by a model-based refinement approach [21] that used the three-dimensional reconstruction of rhesus rotavirus [28] as the initial model. To optimize the search procedure, calculations were performed using only a portion of the Fourier transform of the masked image (between 1/70 Å-1 and 1/30 Å-1) to remove both low- and high-frequency noise. The translation (x,y) and orientation (0,0,w) parameters were refined for each particle by use of repeated cycles of correlation procedures [29, 30, 20, 21]. Images were typically discarded if they showed a correlation coefficient, calculated between the raw image and the corresponding projected view of an intermediate reconstruction, greater than one standard deviation below the mean coefficient of the entire data set.

The final maps were computed based on a total of 260, 165, and 484 individual particles of nucleoprotein components, natural top component, and artificial empty capsids, respectively.

Encapsulation of Fluorescent Dyes within CPMV Capsids

Five milligrams of virus (T, MIX, or AT components) were incubated with 200× excess of either fluorescein 5-maleimide, MIANS (Molecular Probes), or Cy5 maleimide (Amersham Pharmacia) in a solution mixture of 10% DMSO and 90% phosphate buffer (pH 7.0) at room temperature in a total reaction volume of 100 μl. The reactions were incubated for 18–24 hr at room temperature. After the reaction, the excess dye was removed by two rounds of ultracentrifugation on 10%–40% sucrose gradients. The fluorescent bands corresponding to the modified virus were collected and diluted with phosphate buffer. The derivatized virus was recovered by ultracentrifugation. The amount of dye attached was determined by measuring the absorbance of dye-modified virus samples at 495 nm (fluorescein 5-maleimide), 320 nm (MIANS), or 650 nm (Cy5). Virus concentration was measured by determining the absorbance at 260 nm. The concentration of the virus at 0.1 mg/ml in the sample thickness of 1 cm corresponds to an OD reading of 0.8. Each data point was obtained from the average of three independent, parallel reactions, which were repeated at least three times. The typical variation was 5%–15%.

Acknowledgments

W.F.O. thanks Lipika Basumallick for helpful discussions. The authors wish to acknowledge support from the NIH (grant R01EBB00432 02 to J.E.J.) and the Office of Naval Research (grants N00014-00-1-0671 to J.E.J. and N00173-01-C2012 to T.L.).

Received: March 15, 2006
Revised: May 18, 2006
Accepted: May 19, 2006
Published: July 28, 2006

References

1. Douglas, T., and Young, M. (2006). Making friends with old foes. Science *312*, 873–876.
2. Douglas, T. (2003). A bright bio-inspired future. Science *299*, 1192–1193.
3. Peabody, D.S. (2003). A viral platform for chemical modification and multivalent display. J. Nanobiotechnology *1*, 5–12.
4. Chen, C., Daniel, M.-C., Quinkert, Z.T., De, M., Stein, B., Bowman, V.D., Chipman, P.R., Rotello, V.M., Kao, C.C., and Dragnea, B. (2006). Nanoparticle-templated assembly of viral protein cages. Nano Lett. *6*, 611–615.
5. Chen, C., Kwak, E.S., Stein, B., Kao, C.C., and Dragnea, B. (2005). Packaging of gold in viral capsids. J. Nanosci. Nanotechnol. *12*, 2029–2033.
6. Radloff, C., Vaia, R.A., Brunton, J., Bouwer, G.T., and Ward, V.K. (2005). Metal nanoshell assembly on a virus bioscaffold. Nano Lett. *5*, 1187–1191.
7. Dragnea, B., Chen, C., Kwak, E.S., Stein, B., and Kao, C.C. (2003). Gold nanoparticles as spectroscopic enhancers for in vitro studies on single viruses. J. Am. Chem. Soc. *125*, 6374–6375.
8. Lomonossoff, G.P., and Johnson, J.E. (1991). The synthesis and structure of comovirus capsids. Prog. Biophys. Mol. Biol. *55*, 107–137.
9. Wang, Q., Lin, T., Tang, L., Johnson, J.E., and Finn, M.G. (2002). Icosahedral virus particles as addressable nanoscale building blocks. Angew. Chem. Int. Ed. Engl. *41*, 459–462.
10. Wang, Q., Kaltgrad, E., Lin, T., Johnson, J.E., and Finn, M.G. (2002). Natural supramolecular building blocks. Wild-type cowpea mosaic virus. Chem. Biol. *9*, 805–811.
11. Chatterji, A., Ochoa, W., Shamieh, L., Salakian, S.P., Wong, S.M., Clinton, G., Ghosh, P., Lin, T., and Johnson, J.E. (2004a). Chemical conjugation of heterologous proteins on the surface of cowpea mosaic virus. Bioconjug. Chem. *15*, 807–813.
12. Chatterji, A., Ochoa, W.F., Paine, M., Ratna, B.R., Johnson, J.E., and Lin, T. (2004b). New addresses on an addressable virus nanoblock; uniquely reactive Lys residues on cowpea mosaic virus. Chem. Biol. *11*, 855–863.
13. Blum, A.S., Soto, C.M., Wilson, C.D., Cole, J.D., Kim, M., Gnade, B., Chatterji, A., Ochoa, W.F., Lin, T., Johnson, J.E., et al. (2004). Cowpea mosaic virus as a scaffold for 3-D patterning of gold nanoparticles. Nano Lett. *4*, 867–870.
14. Blum, A., Soto, C., Wilson, C., Brower, T.L., Steven, P., Schull, T., Chatterji, A., Lin, T., Johnson, J., Amensick, C., et al. (2005). An engineered virus as a scaffold for three-dimensional self-assembly on the nanoscale. Small *1*, 702–706.
15. Chatterji, A., Ochoa, W.F., Ueno, T., Lin, T., and Johnson, J.E. (2005). A virus-based nanoblock with tunable electrostatic properties. Nano Lett. *5*, 597–602.
16. Falkner, J., Turner, M., Bosworth, J., Trentler, T., Johnson, J., Lin, T., and Colvin, V. (2005). Virus crystals as nanocomposite scaffolds. J. Am. Chem. Soc. *127*, 5274–5275.
17. Shanks, M., and Lomonossoff, G.P. (2000). Co-expression of the capsid proteins of cowpea mosaic virus in insect cells leads to the formation of virus-like particles. J. Gen. Virol. *81*, 3093–3097.
18. Douglas, T., Strable, E., Willits, D., Aitouchen, A., Libera, M., and Young, M. (2002). Protein engineering of a viral cage for constrained nanomaterials synthesis. Adv. Mater. *14*, 415–418.
19. Zhao, X., Fox, J.M., Olson, N.H., Baker, T.S., and Young, M.J. (1995). In vitro assembly of cowpea chlorotic mottle virus from coat protein expressed in *Escherichia coli* and in vitro-transcribed viral cDNA. Virology *207*, 486–494.
20. Baker, T.S., Newcomb, W.W., Olson, N.H., Cowsert, L.M., Olson, C., and Brown, J.C. (1991). Structures of bovine and human papillomaviruses. Analysis by cryoelectron microscopy and three-dimensional image reconstruction. Biophys. J. *60*, 1445–1456.
21. Baker, T.S., Olson, N.H., and Fuller, S.D. (1999). Adding the third dimension to virus life cycles: three-dimensional reconstruction of icosahedral viruses from cryo-electron micrographs. Microbiol. Mol. Biol. Rev. *63*, 862–922.
22. Wellink, J. (1998). Comovirus isolation and RNA extraction. Methods Mol. Biol. *81*, 205–209.
23. Lin, T., Schildkamp, W., Brister, K., Doerschuk, P.C., Somayazulu, M., Mao, H.K., and Johnson, J.E. (2005). The mechanism of high-pressure-induced ordering in a macromolecular crystal. Acta Crystallogr. D Biol. Crystallogr. *61*, 737–743.
24. CCP4 (Collaborative Computational Project, Number 4) (1994). The CCP4 suite: programs for protein crystallography. Acta Crystallogr. D Biol. Crystallogr. *50*, 760–763.
25. Lin, T., Chen, Z., Usha, R., Stauffacher, C.V., Dai, J.B., Schmidt, T., and Johnson, J.E. (1999). The refined crystal structure of cowpea mosaic virus at 2.8 Å resolution. Virology *265*, 20–34.
26. Booy, F.P., Newcomb, W.W., Trus, B.L., Brown, J.C., Baker, T.S., and Steven, A.C. (1991). Liquid-crystalline, phage-like packing of encapsidated DNA in herpes simplex virus. Cell *64*, 1007–1015.
27. Carrascosa, J.L., and Steven, A.C. (1978). A procedure for evaluation of significant structural differences between related arrays of protein molecules. Micron *9*, 199–206.
28. Yeager, M., Dryden, K.A., Olson, N.H., Greenberg, H.B., and Baker, T.S. (1990). Three-dimensional structure of rhesus rotavirus by cryoelectron microscopy and image reconstruction. J. Cell Biol. *110*, 2133–2144.
29. Baker, T.S., Drak, J., and Bina, M. (1988). Reconstruction of the three-dimensional structure of simian virus 40 and visualization of the chromatin core. Proc. Natl. Acad. Sci. USA *85*, 422–426.
30. Fuller, S.D. (1987). The T=4 envelope of Sindbis virus is organized by interactions with a complementary T=3 capsid. Cell *48*, 923–934.